5J.14 OBSERVATIONS OF THE 24 JUNE 2003 BOW ECHO CASE DURING BAMEX

Dustin Phillips[1] and Kevin Knupp
Department of Atmospheric Science
University of Alabama Huntsville

1. INTRODUCTION

In the late 1970s the convective system that is referred to as the bow echo was identified by Fujita (1978). It was identified as a type of convective storm structure associated with intense damaging winds or downburst (Johns 1993). As more of these systems were studied, a better understanding was made on their kinematic structure and dynamical processes. Bow echoes can range in size from 15 km to 150 km, and can occur at anytime of year (Klimowski et al. 2000). Much of the damage reported in the United Sates from non-tornadic winds is a result of bow echo systems.

The "model" bow echo evolves from a single or large group of strong convective cells, to a bow-shaped line segment, and finally, to a comma-shaped echo in its declining phase (Fujita, 1978). The development of a bow echo can be related to a number of different synoptic variables and conditions. Strong bow echoes that produce widespread damage can occur in strong migrating low pressure systems as well as in rather benign synoptic patterns.

During the Bow Echo and MCV Experiment (BAMEX) the ground-based platforms – the Mobile Integrated Profiling System (MIPS) and two NCAR MGLASS units – were deployed in advance of evolving mesoscale convective systems to monitor the environmental and storm properties of bow echo systems.

On 24 June 2003 the MIPS was deployed at a site just south of Fort Dodge in Northwest Iowa, about 86 km from the Des Moines (DMX) WSR-88D radar. The NCAR MGLASS1 was deployed 76km to the west, and MGLASS2 was 176 km to the north. Around 0650 UTC, the MIPS acquired an excellent data set on a surging bow echo near the time of maximum radial velocity (exceeding 30 m s^{-1}) measured from the DMX WSR-88D The peak updraft within deep convection, ~20 m s^{-1}, occurred about 10 minutes after the gust front arrival. The maximum surface wind gust of 24 m s^{-1} was measured about 10 minutes after the gust front arrival, well behind the leading edge within relatively heavy precipitation.

The goals of this paper are (1) to analyze MIPS data to define the environment preceding the bow echo (GLASS soundings and the radiometer (MPR)), and to describe the environment in the wake of the bow echo; and (2) to describe the internal storm structure from an analyses of MIPS 915 MHz profiler and electric field mill measurements, MPR measurements, ceilometer measurements, supplemented with Doppler analyses from the DMX WSR-88D and the NCAR Eldora airborne Doppler radar.

*Corresponding authors address: Dustin Phillips, 320 Sparkman Dr. NSSTC, Huntsville, AL 35805; email phillips@nsstc.uah.edu

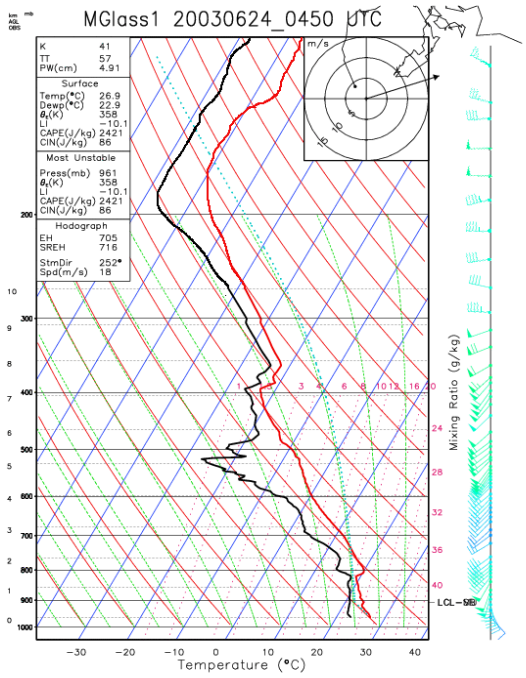

Figure 2.1.1 Skew-T sounding plot from the MGLASS 1 location at 0450 UTC on 24 June. This sounding was release 76 km from the MIPS location. The CAPE value was 2421 J kg-1, with a surface lifted index 0f -10.1, indicating an unstable air mass at this time.

2. STORM ENVIRONMENT

2.1 Composite Sounding

Figure 2.1.1 displays a skew-T plot from MGLASS1 at 0450 UTC. This sounding was launched about two hours before arrival over the MIPS and one hour before passing over the MGLASS1 location. This sounding original went to 300 hPa, however using soundings from other NWS sites in the region as well as the 915 MHz profiler and the Slater, IA 404 MHz Profiler the sounding was able to be completed up to the tropospheric level. A shallow mixed layer extends from the surface to 925 hPa. Above this, a moist adiabatic layer is capped by a stable layer centered near 800 hPa. The MCS anvil cloud base is apparent near 400 hPa, and precipitation

evaporation is suggested from anvil base to about 470 hPa. From this sounding the CAPE value is calculated to be near 2400 J kg^{-1}. This value matches well with surrounding NWS soundings as well as soundings from the MIPS MPR. It is interesting to note that in Johns (1993) it was found that the average CAPE value for bow echo systems was near 4500 Jkg^{-1}. However in this case the CAPE values only reached values of 2400 J kg^{-1}, which is far from the 4500 J kg^{-1} that was found in past studies to be an optimal value for these types of systems. To the south the CAPE values were much larger, in some cases exceeding the 4500 J kg^{-1}. To the north in Minnesota the CAPE values were lower than in Iowa, regardless the convection continued to mature and move eastward in the lower CAPE environment. The lifted index for a surface-based parcel is appreciable at about -10 °C. Veering and speed shear is most significant below 850 hPa. Middle tropospheric flow is uniform southwesterly near 25-30 m s^{-1}, and overlies a low level jet of 25 m s^{-1}, centered near 1 km AGL.

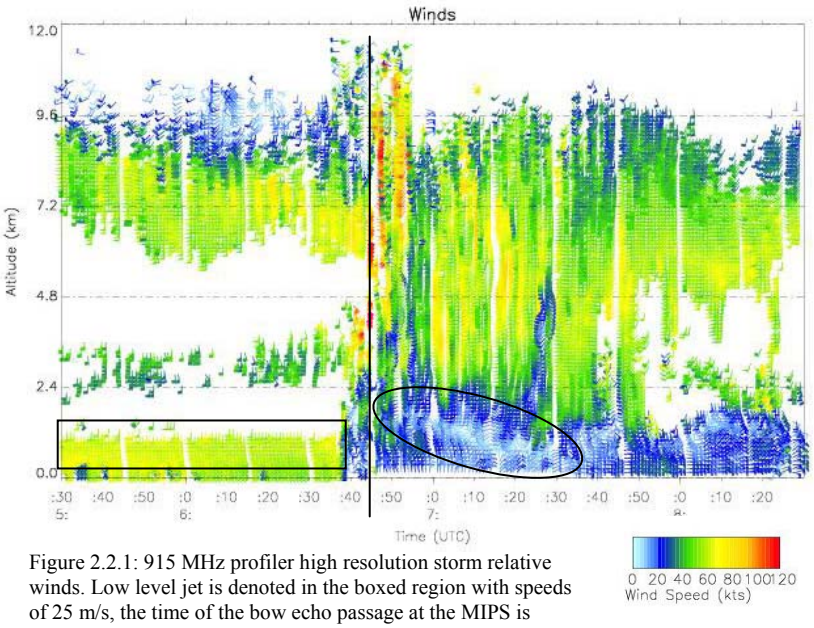

Figure 2.2.1: 915 MHz profiler high resolution storm relative winds. Low level jet is denoted in the boxed region with speeds of 25 m/s, the time of the bow echo passage at the MIPS is shown by the black line. The rear inflow jet is located within the circular area.

2.2 Boundary Layer Part 1 – 915 MHz Profiler

A time vs. height section of horizontal flow from the 915 MHz profiler is shown in figure 2.2.1. The high resolution winds have been unfolded as well as converted to storm relative winds. The figure reveals three prominent features: 1) A low level jet (25 m s^{-1}) exists near 1 km AGL. This jet was also present in the MGLASS sounding from 0450 UTC. 2) Strong southwesterly midlevel flow of 25 m s-1 was sampled at the back of the system, but this jet did not descend to low levels. 3) The most significant wind change was confined to the lowest 2 km, where strong southerly winds (and the southerly jet near 1 km AGL) were replaced by weaker northerly flow.

The inversion layer shown in the MGLASS1 sounding is also visible as enhanced return power (SNR) from the 915 MHz profiler, shown in time-height section format in Fig. 2.2.2. At 0520 UTC, layers of enhanced SNR are located near 1.5, 2.0 and 3.5 km. Enhanced SNR over the lowest 1 km was produced by Rayleigh scatter from insects. The layer at 2 km

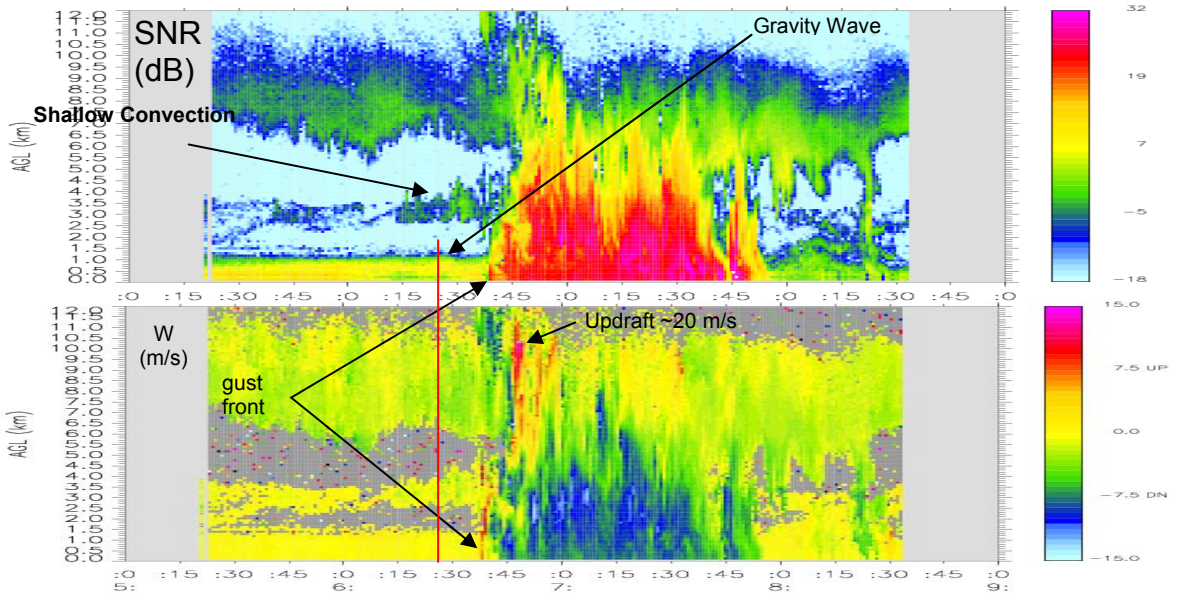

Figure 2.2.2: MIPS 915 MHz SNR and Vertical Velocity

corresponds to the inversion near 800 hPa (MGLASS1 sounding) and was produced by Bragg scatter. This layer moved upward to 2.5-3.0 km by 0540, suggesting that the environment changed rapidly in advance of the bow echo. By 0615 UTC, a deeper layer of enhanced SNR (indicative of shallow convective structures) had developed within the 2.5-4.0 km layer, suggesting lifting and associated destabilization immediately in advance of the bow echo. This destabilization shown by the SNR can be correlated to an increase in the vertically integrated vapor (VINT), and vertical integrated liquid (LINT) measured by the MPR for the same time period (figure 7). For this time period the VINT increased by approximately 0.6 cm, as well as the LINT showing increases of approximately 1 mm as the shallow convection developed ahead of the system. This increase is an indication that the atmosphere was destabilizing, which in turn could support the shallow convection measured by the 915 MHz profiler.

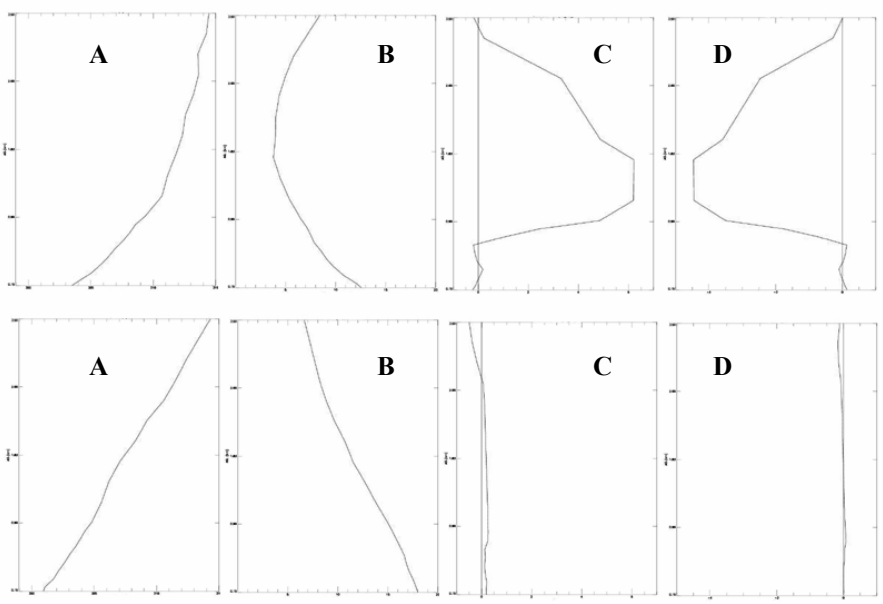

Figure 2.3.1 Vertical profiles of (a) Potential Temperature (θ) (k), (b) Mixing Ration (q) (g/g), (c) Heat Flux (w´θ´), and (d) Mixing Ratio (q´w´) for 0536 UTC (top) and 0635 UTC (bottom). Vertical Scale is from surface to 3.5 km.

2.3 Boundary Layer 2 - Nocturnal Parameters

The nocturnal boundary layer (NBL) has often been overlooked in studies of squall lines, bow echoes, MCS, and other nighttime weather systems because of the complexity associated with it. However, many studies have used parameters that work during the daytime hours to explain nighttime phenomena even though the NBL has many different characteristics than the convective boundary layer (CBL). The 24 June case occurred during the late night hours well after the NBL has setup over the domain. Roland Stull in his book "An Introduction to Boundary Layer Meteorology" states that the NBL is difficult to describe and model and that it is very complex in nature. There are many different types of NBL structures which make it difficult to classify what type occurs on any given night. For this paper 4 main NBL quantities, moisture flux (q´w´), heat flux (w´θ´), mixing ratio (q), and potential temperature (θ) will be briefly analyzed to better understand the NBL and how it relates to bow echo development, growth, and decay.

To calculate these parameters the 915 Profiler and the MPR were used from 0530 – 0640 UTC. Vertical motion is measured directly from the 915 1st moment. However the other parameters can not be found directly from measurements of the MPR and 915. In calculating all values 21 levels were used from the surface to 3.5 km AGL. These levels were broken into the following heights: from the surface to 1 km, .10km spacing, from 1km to 3.5 km, .25 km spacing. These levels are based on the resolution of the MPR. To be able to calculate the fluxes the MPR and 915 had to be placed into the same time space format. This was done by averaging the 915 gates to match the MPR spacing, and then averaging both data sets to the same time periods.

Figure 2.3.1 shows a vertical profiles of θ, q, w´θ´, and q´w´ for 0536 UTC and 0635 UTC. From these parameters it is clear that the NBL depth at 0536 is approximately between 700-800m. The NBL depth remained approximately the same for both profiles. It is interesting to note that there are large fluxes in both heat and moisture ahead of the system, but as it was nearing these fluxes went basically to zero. The mixing ratio values increased in the NBL from 0536 to 0635 UTC by nearly from 13 kg/kg to 18 kg/kg as the bow was approaching. It also increased in the upper levels by a smaller amount. Theta increased slightly over this period between the surface and 2 km, but remained the same above this level. These profiles show that the NBL was not growing in depth but it was becoming more stable as the system approached. This analysis has brought new insight into the pre-bow environment, which consisted of many waves, along with a gravity wave that was measured by the MIPS instruments and WSR-88D Radar. This Nocturnal Boundary Layer can be classified as mixed, with a residual layer occurring up to 3.5 km. Waves were forming within the system and racing out ahead of the leading edge which was causing oscillations in the inversion layer. This boundary layer was changing rapidly, which is shown by theta, as well as the heat flux, and moisture flux plots.

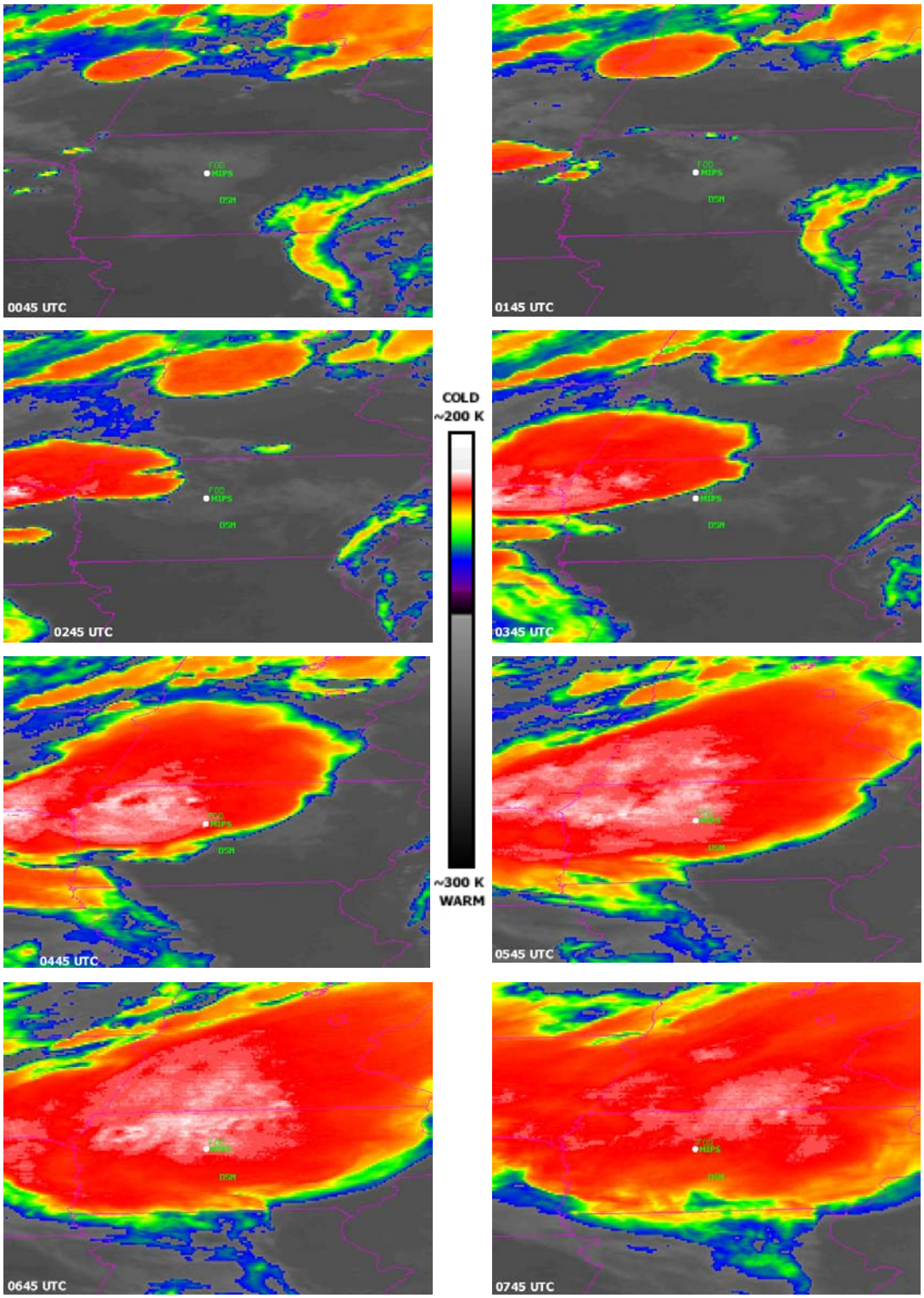

Figure 3.1.1 GOES-12 4-km resolution infrared images from 0045 – 0745 UTC. The locations of the cities of Fort Dodge, IA (FOD), and Des Moines, IA (DSM), as well as the MIPS location have been superimposed. Starting from the top right the cells initiate over South Dakota and mature as they move to the south and east over across Iowa. The coldest cloud tops pass over the MIPS location between 0545 and 0745 UTC.

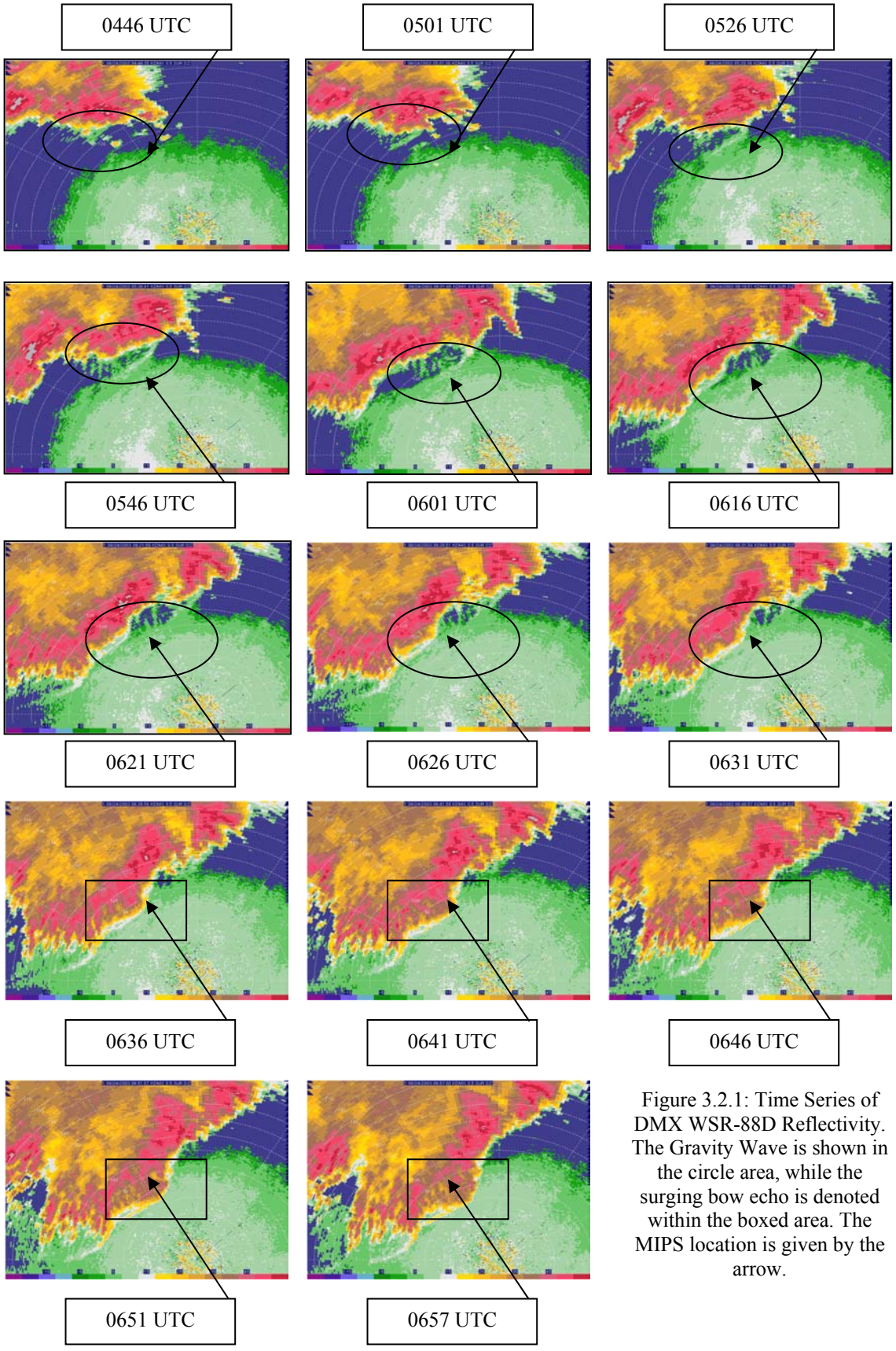

Figure 3.2.1: Time Series of DMX WSR-88D Reflectivity. The Gravity Wave is shown in the circle area, while the surging bow echo is denoted within the boxed area. The MIPS location is given by the arrow.

3. STORM STRUCTURE

3.1 GOES Infrared Sequence

Figure 3.1.1 shows a series of GOES-12 infrared images from approximately the time of convective initiation until 1 hour after the passage of the system over the MIPS. All images have a 4-km resolution. The IR values range from 300 K (denoted by black and gray), to 200 K (denoted by white). Approximately 5 hours prior to the passage over the MIPS the system began to form over Nebraska and South Dakota. This is clearly shown at 0045 UTC as a small cluster of cells forming over southern South Dakota and Northern Nebraska. There are at this time high cirrus clouds covering most of central Iowa, with clear conditions over Southern Minnesota and Northern Missouri. One hour later the cells have become more numerous and the coverage area has gown considerably. At 0245 UTC the cloud tops begin to cool considerably to values near 200 K over Nebraska. At this time the system begins to combine and form into a squall line. During the next two hours the system continues to mature and intensify, shown by the cloud top temperatures cooling and expanding in coverage. Between 0445 and 0545 UTC the system begin to take the shape of a common bow echo system as it begins to race towards the east and south across Iowa. The anvil of the system is now large covering most of Iowa and Southern Minnesota. At 0645 UTC, as the system passes over the MIPS, the coldest cloud tops are present as well as the strongest radial velocity winds recorded with this system. Finally, after the passage the cloud top temperatures begin to rises as the system begins to decay and fall apart. The system also begins to lose the well defined cloud shield on the southern and southeastern edge. Cloud tops do however remain cold in Minnesota where convection continues to mature and move eastward.

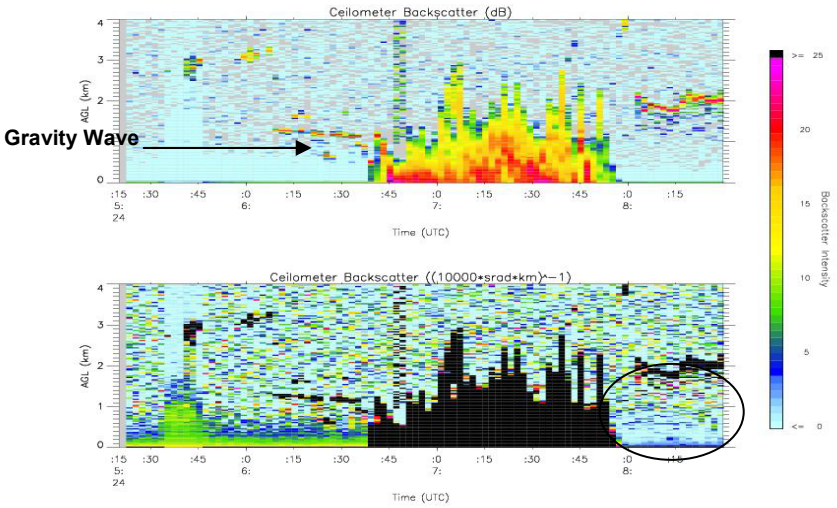

Figure 3.3.1: Time Height Series of MIPS Ceilometer. The top panel is ceilometer backscatter in units of dB. The bottom panel is backscatter in units of power. Heavy rain is denoted by the black color. The area in the circle shows how the atmosphere became more pristine after the passage of the bow.

3.2 Des Moines WSR-88D

The sequence of PPI images in Figure 3.2.1 presents a sequence of radar reflectivity images from the DMX WSR-88D for a 2-h period around the time of passage over the MIPS. This figure shows a gravity wave, outflow boundary, along with the evolution of the bow echo prior to and after the arrival over the MIPS. The mesoscale organization of the MCS changed significantly over this period, from an orientation of west to east at 0446 UTC, to southwest to northeast by 0646 UTC. The initial bulge in the bow echo appeared around 0616 UTC and became prominent by 0641 UTC, near the time of passage over the MIPS. At 0446 UTC a gravity wave emerged from the main cell along the squall line. This gravity wave denoted in the circular area was sampled well by the WSR-88D Radar. As the gravity wave moved away from the system to the southeast it began to diffuse and was no longer measurable at 0630 UTC. This was the case because the atmosphere was not contusive for ducting of waves. So the gravity wave was not able to sustain for a longer period of time. At 0621 a gust front emerged from the leading edge of precipitation, and accelerated ahead of the system. The gust front was sampled by the MIPS 17 min later at 0638, and is marked by a fine line in the 915 SNR, and a narrow updraft in the 915 vertical velocity field. As the system neared the MIPS location it began to form an apex and at the same time the radial velocity signature of the storm reached the highest values recorded for the southern portion of the system. This apex is shown in the boxed area in figure 5.2.1. Soon after the passage over the MIPS the system began to decay and by 0800 UTC there were only a few isolated cells remain. However, there was a strong outflow boundary pushing across central Iowa initiating small cells along the leading edge.

3.3 MIPS Observations

The bow echo core between 0645 and 0710 UTC is depicted by large values of 915 SNR in Fig. 2.2.2, and high values of ceilometer backscatter in Fig. 3.3.1. A low-level updraft of about 10 m s-1, confined to below 2.5 km, accompanied the sharp gust front sampled near 0638 UTC. A clear signature of the gust front passage is revealed in the surface measurements (Fig. 3.3.2), which reveals sharp wind shift and temperature drop. The gust front updraft preceded the storm core updraft, shown as several maxima within the 4-12 km AGL altitude range. The maximum updraft is

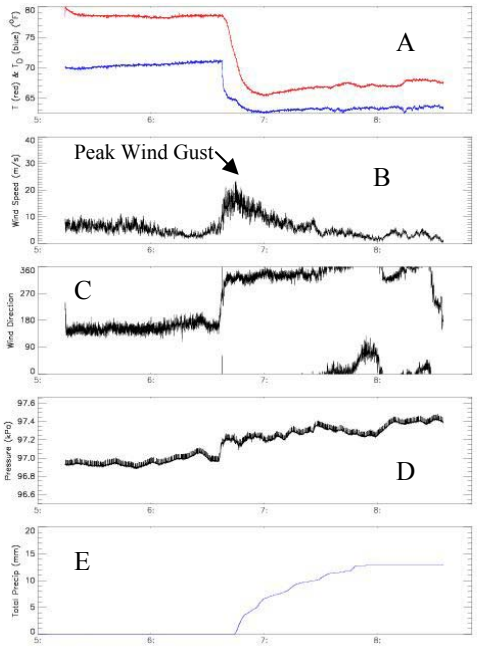

Figure 3.3.2: MIPS surface time series. (a) Temperature is red, Dewpoint blue (b) Wind speed (m s^{-1}) (c) Wind direction (d) Pressure in kPa (e) Total Precipitation

estimated at ~20 m s^{-1} near 10.5 km at 0645-0650 UTC. (Fig. 2.2.2). The maximum wind gust of 24 m s^{-1} occurred at approximately 0652 which corresponds will the distinct maxima in negative W near the 2.5 km level at 0652. Other distinct wind gusts at 0659 (16 m s-1) and 0707 (13 m s^{-1}) were also recorded and correspond well with maxima in negative W at 0659 and 0707 UTC.

During this project the MIPS was equipped with a JOSS-WALDVOGE disdrometer which was able to determine the drop size distribution which can be used with the 915 MHz Profiler to determine the vertical air motions within the bow echo system. The disdrometer also allows for refractivity values to be determined using the 915 data. Figure 3.3.3 shows the refractivity time series as well as the air motion time series from this case. If the terminal fall speed for rain is assumed (hail was not observed at the surface) and using the relation, $w = W - V_T$, in which W is measured Doppler velocity (vertical incidence) and V_T is terminal fall speed we can calculated the air motion. However, for this system there was grapel present in the upper portion of the system above the freezing level. At this time air motion above this level can not be accurately determined, work is on going here to solve this problem. The figure does however show the air motion from the surface to just above 5 km. The largest value of upward motion was found to be right after the initial passage of the system at 0645 UTC. The highest upward motion recorded was 15 m/s, while the largest downward motion measured was 5m/s. As for the refractivity the highest value was 56 dBZ during the initial deep convection at 0652 UTC.

The electric filed mill (EFM) time series (Fig.3.3.4) provides valuable information on storm properties based on measurements of the vertical component of the electric field, sampled at a rate high enough (50 Hz) to resolve lightning flashes. Local lightning flashes are represented as discontinuities (quasi-vertical lines) in the time series, and appear at frequent intervals, particularly within the bow echo core. Mesoscale features and subtle variations in the E field

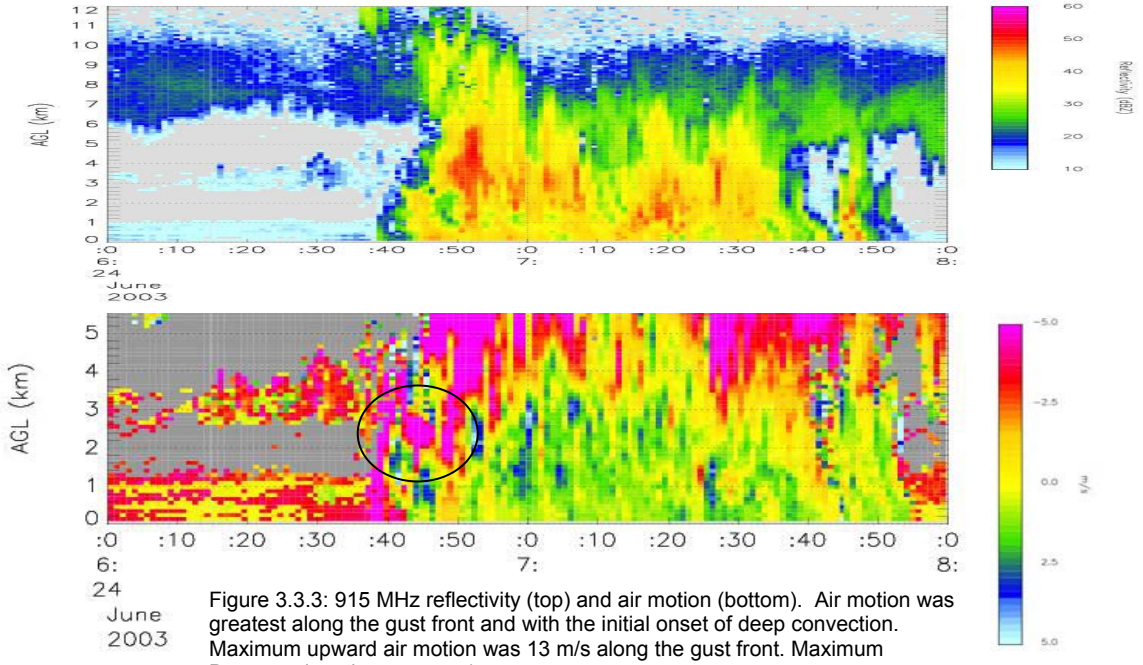

Figure 3.3.3: 915 MHz reflectivity (top) and air motion (bottom). Air motion was greatest along the gust front and with the initial onset of deep convection. Maximum upward air motion was 13 m/s along the gust front. Maximum Downward motion was -5m/s.

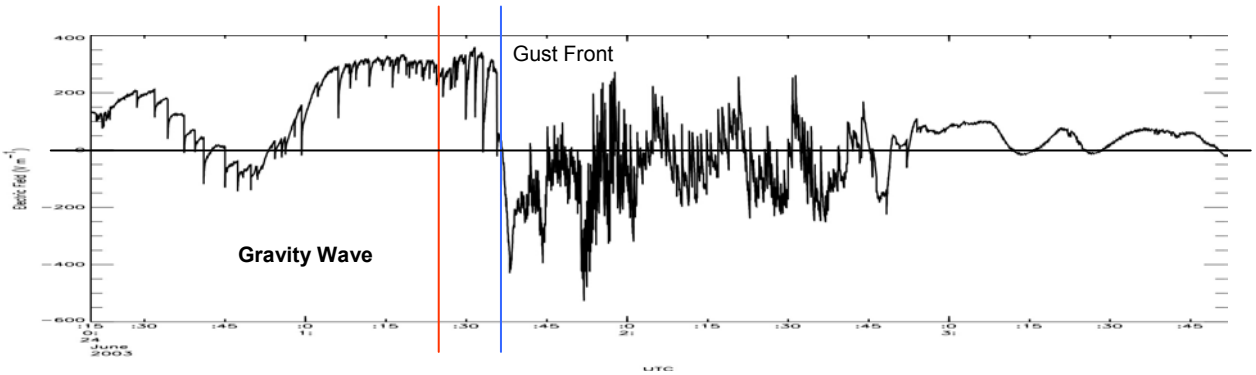

Figure 3.3.4: MIPS EFM Time Series. The gravity wave passage is denoted by the red line and gust front passage by the blue line. The neutral line is the black line across the time height series. Positive charge is above that line, and negative below it.

are apparent in several locations: a gravity wave passage at 0620, the gust frontal passage at 0638 UTC and electric field oscillations near the trailing portion, and within the wake, of the receding and weakening bow echo. Coupling this data with data from the National Lightning Detection Network (NLDN) data the total lightning flash count can be determined. For this analysis a radius of 10 km around the MIPS EFM was used. For the period of 0515 UTC to 0845 UTC there was approximately a total of 240 lightning flashes in the area of study. There were 98 cloud to ground flashes and 142 inter-cloud flashes. Overall the flash rate was low with this system, with an average flash rate of 1.2 flashes per minute over the entire time series and a rate of 2.6 flashes per minute during deep convection.

The microwave profiling radiometer (MPR) data, depicts relative variations in thermodynamic structure in non precipitating regions before and after storm passage. The MPR acquires soundings at high temporal resolution of 1 minute, but vertical resolution scales with height (i.e., greatest vertical resolution is near the surface). The MPR measured an increase in vertically integrated values of water vapor and cloud water prior to arrival of the bow echo, which is consistent with the 915 backscatter evolution also shown in figure 2.2.2. Cooler and drier air was measured in the wake of the bow echo after 0715 UTC (when the radome water coating evaporated) which is shown by the lower values of relative humidity in the lower part of the atmosphere.

3.4 Cold Pool Analysis

Over the past few decades there have been several idealized numerical modeling studies that have shown a relationship between the structure of a mesoscale convective system (MCS) and a non-dimensional parameter relating cold pool strength to environmental wind shear. One goal of BAMEX was to move forward from a numerical study to an observation

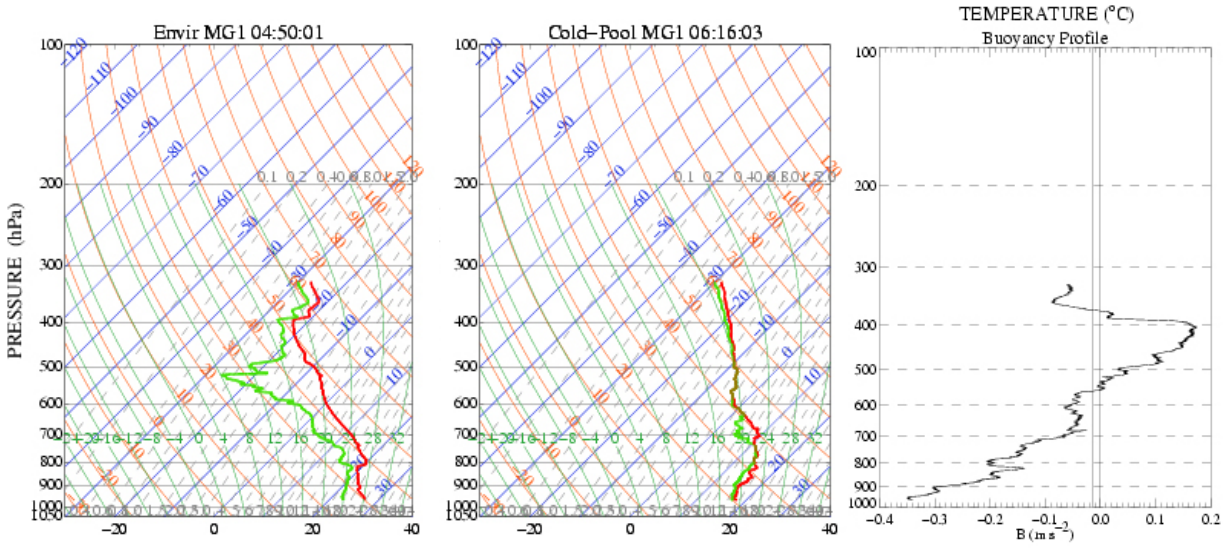

Figure 3.4.1: Cold Pool Analysis. Environmental sounding released at 0450 UTC, cold-pool sounding released at 0616, and the buoyancy profile for this system.

study of the cold pool. To conduct an analysis at least two soundings are needed: one in the undisturbed environment ahead of the system, and one in the system's cold pool. For this case there were a total of four soundings that fit the criteria for doing this analysis. The environmental sounding was released at 0450 UTC from MGLASS1. The cold pool sounding was released at 0616 from the same location as the previous sounding. These two soundings are shown in figure 3.4.1.

The environmental sounding was released in an environment that had not been disturbed by convection, but it was released as the NBL was maturing. The cold pool sounding was released in the middle of the convective region near the end of the precipitation. The trailing stratiform line weakens rapidly after passing the M_Glass1 Site. The cold pool sounding also shows the melting layer to be approximately 610 mb (4256 m). By analyzing these soundings the cold pool parameters can be found. For this case the buoyancy profile is negative from the surface to 557 mb. The strength of the system's surface-based cold pool, measured by C was found to be 35.71 m/s. The low- to mid-level vertical wind shear in the environment, measured by ΔU, was found to be 9.89 m / s. Past studies such as Rotunno et al. (1988) and Weisman et al. (1988) have stated that when C > ΔU the cells tend to lean up shear and when C < ΔU the cell tend to lean down shear. Model simulations typically produce a trailing stratiform system when C > ΔU. However, in this case little to no stratiform precipitation occurred with the southern end of the system. There is some suggestion that weakening systems tend to have C >> ΔU, while mature and intensifying tend to have a C / ΔU ratio closer to 1 Bryan et al. (2004). In this case the system did decay rapidly after moving through the domain.

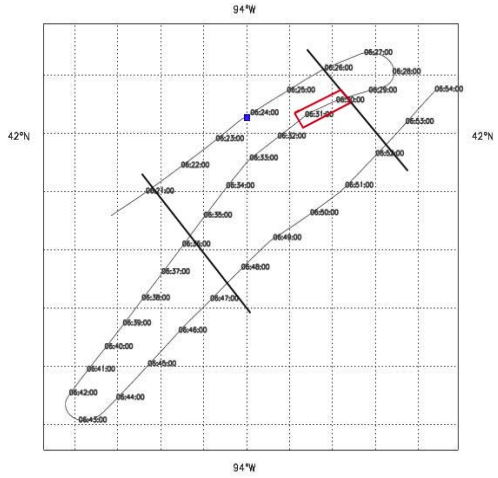

Figure 3.5.1: Flight Track of the Eldora (MIPS is located in the blue square) (Leg 1 is the top track, Leg 2 middle, and Leg 3 bottom track)

3.5 Eldora Observations

For the 24 June 2003 case the NRL-P3 and the NOAA P-3 both deployed in the same area as the ground crew. However the NOAA P-3 experienced an engine failure on route to the targeted area. For this case the radar data from the Eldora forward and aft tail radar will be analyzed. Figure 3.5.1 shows the track of

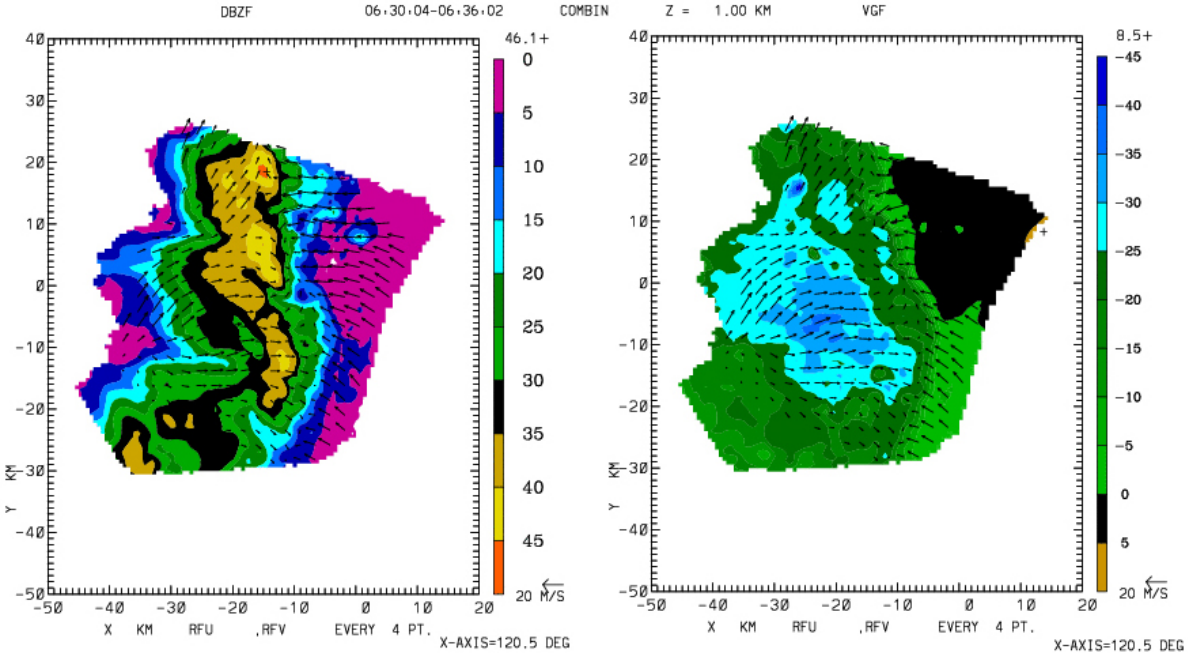

Figure 3.5.2 Eldora reflectivity and velocity plots for leg2. The dual doppler wind vectors are overlaid on both plots in m/s. The MIPS is located at the coordinates (0, 0).

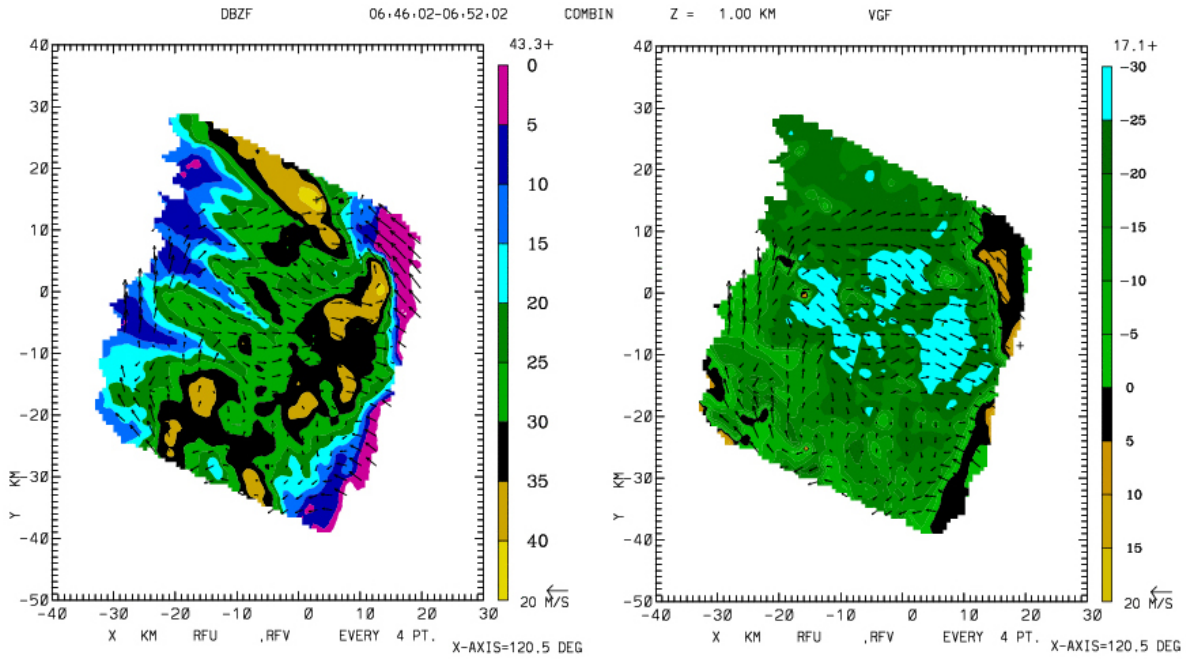

Figure 3.5.3 Eldora reflectivity and velocity plots for leg3. The dual doppler wind vectors are overlaid on both plots in m/s. The MIPS is located at the coordinates (0, 0). Notice that the system has weakened considerably between the two legs.

the P-3 in reference to the MIPS location. For this case there are a total of three legs that are relevant to use for a comparison with MIPS measurements and for grasping a better understanding of the structure of the bow echo system. For this paper, scans from legs 2 and 3 will be analyzed. Figure 3.5.2 shows a scan from the Eldora fore radar as it passed near the MIPS during the bow echo passage. The left panel is reflectivity in units of dBZ and the right panel is the unfolded and corrected radial velocity data with the dual Doppler winds overlaid. This scan is a slice taken at Z=1 km during leg2 which correlates to the time the bow was approaching the MIPS. The surging portion is shown will velocities of -30 m s-1 along the edge of the system, with higher values approaching -40 m s-1. The reflectivity shows the apex of bowing segment beginning to form just west of the MIPS position. Recalling from earlier in the paper the 915 MHz Profiler showed a low level jet (25 m s^{-1}) that existed near 1 km AGL This same rear inflow jet is shown in the reflectivity and velocity data. In the reflectivity it is the notch at the rear of the system, and in the velocity it is shown by the dual Doppler winds of approximately 30 m s-1 on the left side of the system.

Figure 3.5.3 shows a scan from the 3rd leg. Again, the left panel is reflectivity in units of dBZ and the right panel is the unfolded and corrected radial velocity data with the dual Doppler winds overlaid. This scan is also a slice taken at Z=1 km. During this leg the MIPS was within an area of deep convection shown by both the Eldora and 915 MHz Profiler (figure 3.3.3). The 915 MHZ Profiler measured reflectivity values of 20-25 dBZ during this leg, while the Eldora scan measured

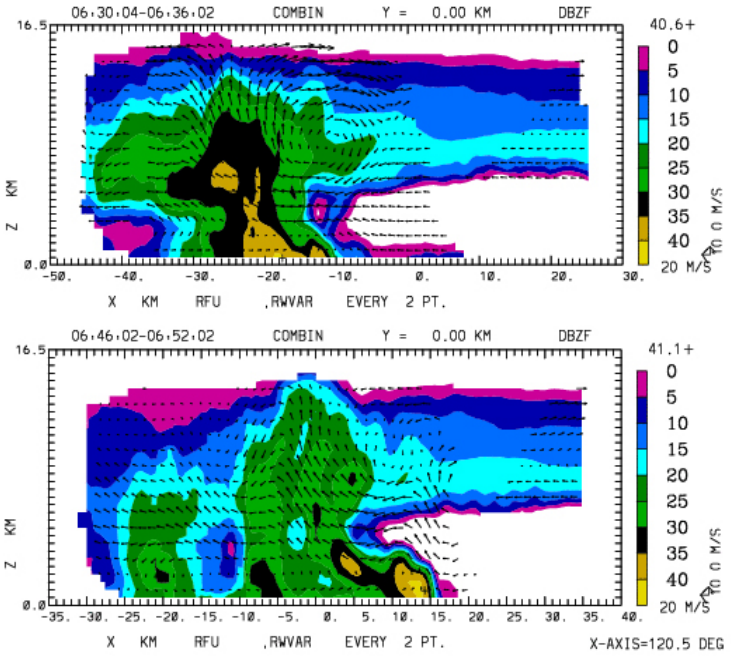

Figure 3.5.4 Vertical cross section from the Eldora Radar. Top panel is during leg 2. Bottom panel is during leg 3. Each scan is taken across the location of the MIPS system, which is located at 0 km on the x-axis.

reflectivity values near 25 dBZ. The velocity values have decreased to values of -30 m s-1 on the high end to values averaging around 10-15 m s-1 within the system.

To further understand the structure of this system a comparison of the Eldora analysis with the 915 storm relative winds (figure 2.2.1) and 915 reflectivity (figure 3.3.3)was completed. Figure 3.5.4 shows a vertical cross section across the MIPS system for leg 2 (top panel) and leg 3 (bottom panel). In both images the MIPS is located at 0 km on the x-axis. As stated above the low level jet is shown ahead of the system in both the Eldora and 915 time series. The magnitudes are approximately the same in both systems. The 915 was measuring reflectivity values between 5-15 dBZ during this leg, which is what the Eldora radar measured over the MIPS at this time. The structure of the system was well sampled with the main updraft showing up well at -10 km from the MIPS system. There was deep convection occurring with the system with reflectivity values reaching as high as 40 dBZ in the main core. However, at this time there was little to no outflow with the system. Values of 10-15 m/s were measured by the Eldora radar system. During the 3rd leg the system had undergone a major transformation from a well organized stage to a decaying stage. This decrease can be attributed to the gust front racing out ahead of the system departing from the main updraft of the system. This is shown by the Eldora analysis as high reflectivity well in advance of the main core of the system.

5. CONCLUSIONS

The Bow echo system on 24 June 2003 that passed over the MIPS system had features not measured before. This system as it was passing over head was weakening, but it was surging with the greatest radial velocity (exceeding 30 m s-1 from the DMX WSR-88D and Eldora Dual Doppler Analysis) as it passed over the MIPS. Several key features have been found in this analysis that include the pre-bow atmospheric state, internal storm structure, an interesting gravity wave that occurred before the bow passage, and post atmospheric structure. From this analysis it can be said that the environment ahead of a bow echo system must have instability, which was the case here, cape values were in the 2500 J kg^{-1} range. The upper level winds must be westerly, there must be sufficient wind shear, and there needs to be a strong low level jet. Looking at the internal structure of the system it was found that the bow echo is made up of several different cells, each having different structure and strength. It was interesting to note that in the stronger portions of the system the electric field was positive, and stronger than the less intense portions of the bow echo. Post atmospheric conditions were much dry, and much more pristine than before the system passed over. This is shown by the MPR and the ceilometer data. This system was not a classic bow echo or the model bow echo because it lacked a large stratiform rain region behind it. However, most system that were studied during BAMEX did not fit into the model bow echo, so that leads to the question, is there a model bow echo? As future research advances hopefully this question can and will be answered. Future work in this area involves further integrating Eldora radar data with the MIPS and MGlass Data as well as further work with the Distrometer data to determine air motion in the upper levels of the system.

7. REFERENCES

George Bryan, David Ahijevych, Chris Davis, Morris Weisman, and Ron Przybylinski, 2004: An assessment of convective system structure, cold pool properties, and environmental shear using observations from BAMEX. Preprints, 22nd Conf. on Severe Local Storms, Hyannis, MA, Amer. Meteor. Soc., CD-ROM, 4.2

Fujita, T. T., 1978: Manual of downburst identification for project NIMROD. Satellite and Mesometeorology Research Paper No. 156, Department of Geophysical Sciences, University of Chicago, 104 pp.

Johns, R.H., 1982: A synoptic climatology of northwest flow severe weather outbreaks. Part 1: Nature and significance. Mon. Wea. Rev., 110, 1653--1663.

Johns, R.H., 1984: A synoptic climatology of northwest-flow severe weather outbreaks. Part 2: Meteorological parameters and synoptic patterns. Mon. Wea. Rev., 112, 449--464.

Johns, R.H., 1993: Meteorological conditions associated with bow echo development in convective storms. Wea. and For., 8, 294-299.

Johns, R.H. and W.D. Hirt, 1987: Derechos: Widespread convectively induced windstorms. Weather and Forecasting, 2, 32--49.

Klimowski, B. A., R. Pyzybylinski, G. Schmocker, and M. R. Hjelmfelt, 2000: Observations of the formation and early evolution of bow echoes. Preprints, 20th Conf. on Severe Local Storms, Orlando, FL, Amer. Meteor. Soc., 44-47.

Rotunno, R., J. B. Klemp, and M. L. Weisman, 1988: A theory for strong, long-lived squall lines. *J. Atmos. Sci.,* **45**, 463–485.

Stull, Roland B. *An Introduction to Boundary Layer Meteorology*. Klumwer Academic Publishers, Boston, 1988.

Weisman, M. L., J. B. Klemp, and R. Rotunno, 1988: Structure and evolution of numerically simulated squall lines. *J. Atmos. Sci.,* **45,** 1990-2013

Weisman, M. L., 1992: The role of convectively generated rear-inflow jets in the evolution of long-lived mesoconvective systems. J. Atmos. Sci., 49, 1826-1847.

Weisman, M.L., 1993: The genesis of severe, long-lived bow-echoes. J. Atmos. Sci., 50, 645-670.

Weisman, M.L. and C. Davis, 1998: Mechanisms for the generation of mesoscale vortices within quasi-linear convective systems. J. Atmos. Sci., 55, 2603-2622.

Morgenstern, C.D., 1991 *Cloud-to-Ground Lightning Characteristics in Mesoscale Convective Systems, April-September 1986*. Master's thesis, Univ. Oklahoma, Norman, 109pp.